Structure
Article

Structural Basis of the PNRC2-Mediated Link between mRNA Surveillance and Decapping

Tingfeng Lai,[1,2,9] Hana Cho,[3,9] Zhou Liu,[4] Matthew W. Bowler,[5,6] Shunfu Piao,[1] Roy Parker,[7] Yoon Ki Kim,[3] and Haiwei Song[1,4,8,*]
[1]Institute of Molecular and Cell Biology, 61 Biopolis Drive, Singapore 138673
[2]School of Biological Sciences, Nanyang Technological University, 50 Nanyang Avenue, Singapore 639798
[3]School of Life Sciences and Biotechnology, Korea University, Seoul 136-701, Republic of Korea
[4]Life Sciences Institute, Zhejiang University, 866 Yuhangtang Road, Hangzhou, China
[5]European Molecular Biology Laboratory, 6 rue Jules Horowitz, BP 181, 38042, Grenoble, France
[6]Unit of Virus Host-Cell Interactions, UJF-EMBL-CNRS, UMI 3265, 6 rue Jules Horowitz, 38042 Grenoble Cedex 9, France
[7]Department of Molecular and Cellular Biology and Howard Hughes Medical Institute, University of Arizona, Tucson, AZ 85721, USA
[8]Department of Biochemistry, National University of Singapore, 14 Science Drive, Singapore 117543
[9]These authors contributed equally to this work
*Correspondence: haiwei@imcb.a-star.edu.sg
http://dx.doi.org/10.1016/j.str.2012.09.009

SUMMARY

Nonsense-mediated mRNA decay (NMD) is an important mRNA surveillance system, and human PNRC2 protein mediates the link between mRNA surveillance and decapping. However, the mechanism by which PNRC2 interacts with the mRNA surveillance machinery and stimulates NMD is unknown. Here, we present the crystal structure of Dcp1a in complex with PNRC2. The proline-rich region of PNRC2 is bound to the EVH1 domain of Dcp1a, while its NR-box mediates the interaction with the hyperphosphorylated Upf1. The mode of PNRC2 interaction with Dcp1a is distinct from those observed in other EVH1/proline-rich ligands interactions. Disruption of the interaction of PNRC2 with Dcp1a abolishes its P-body localization and ability to promote mRNA degradation when tethered to mRNAs. PNRC2 acts in synergy with Dcp1a to stimulate the decapping activity of Dcp2 by bridging the interaction between Dcp1a and Dcp2, suggesting that PNRC2 is a decapping coactivator in addition to its adaptor role in NMD.

INTRODUCTION

Nonsense-mediated mRNA decay (NMD) is an mRNA surveillance pathway that degrades mRNAs harboring premature termination codons (PTCs), thereby preventing the expression of nonfunctional or potentially deleterious truncated proteins in the cell (Amrani et al., 2006; Behm-Ansmant et al., 2007; Chang et al., 2007; Isken and Maquat, 2007; Mühlemann et al., 2008; Rebbapragada and Lykke-Andersen, 2009). In addition to its role in mRNA surveillance, NMD also regulates the stability of a subset of normal mRNAs in diverse eukaryotes (He et al., 2003; Mendell et al., 2004; Rehwinkel et al., 2005; Weischenfeldt et al., 2008; Wittmann et al., 2006).

In yeast, the mechanism by which a PTC is discriminated from a normal stop codon is influenced both by whether the terminating ribosome interacts with the poly(A)-binding protein (PAB1) at the 3′-UTR (Amrani et al., 2006; Mühlemann et al., 2008; Rebbapragada and Lykke-Andersen, 2009) and by other features of the termination context as there is an evidence showing that NMD does not require PAB1 or a poly(A) tail (Meaux et al., 2008). In mammalian cells, recognition of PTCs result from the crosstalk between terminating ribosomes and a downstream *cis*-acting signal known as exon junction complex (EJC), which can include Upf2 and Upf3 (Chang et al., 2007; Isken and Maquat, 2007). If a ribosome encounters a PTC during translation of an erroneous mRNA, it is thought to stall, leading to the formation of a SURF complex, which consists of the SMG1 kinase, Upf1, and two polypeptide release factors eRF1 and eRF3 (Kashima et al., 2006). Subsequently, the interaction of the SURF complex with EJC triggers Upf1 phosphorylation (Kashima et al., 2006) and the decay of the aberrant mRNA is initiated by decapping, deadenylation, and/or endonucleolytic cleavage (Mühlemann and Lykke-Andersen, 2010).

Decapping is a key step in both general (Coller and Parker, 2004; Franks and Lykke-Andersen, 2008) and a number of specialized 5′-to-3′ mRNA decay pathways, including NMD (Amrani et al., 2006; Lejeune et al., 2003), AU-rich element (ARE)-mediated decay (Fenger-Grøn et al., 2005), miRNA-mediated decay (Behm-Ansmant et al., 2006; Eulalio et al., 2007; Song and Kiledjian, 2007), and 3′ uridylation-mediated decay (Rissland and Norbury, 2009; Song and Kiledjian, 2007).

Removal of the cap structure is catalyzed by the decapping enzyme complex, which is composed of the catalytic subunit, Dcp2 and several regulatory proteins acting as both general and pathway-specific decapping activators (Coller and Parker, 2004; Franks and Lykke-Andersen, 2008; Isken and Maquat, 2007; Parker and Sheth, 2007; Parker and Song, 2004). The single subunit enzyme Nudt16 was recently shown to be responsible for decapping of a subset of mRNAs in mammalian cells (Song et al., 2010). In yeast, the general 5′-3′ decay requires the essential activator Dcp1 that directly interacts with Dcp2 and the coactivators, such as Dhh1, the Pat1/Lsm1-7 complex, and the enhancer of decapping proteins Edc1 and Edc2

(Chowdhury and Tharun, 2009; Coller and Parker, 2004, 2005; Sheth and Parker, 2006; Teixeira and Parker, 2007), whereas NMD requires Upf2 and Upf3 to activate decapping (Sheth and Parker, 2006). In humans, the Dcp1/Dcp2 interaction appears weaker and for coimmunoprecipitation from cells requires additional coactivators Edc3, Edc4(Hedls), DDX6/RCK, and TTP in miRNA- and ARE-mediated mRNA decay pathways (Eulalio et al., 2007; Fenger-Grøn et al., 2005).

Dcp1 is a small protein containing an EVH1 domain (She et al., 2004), which is generally a protein-protein interaction module (Ball et al., 2002) through binding to a proline-rich ligand. Recently, Borja et al. (2011) showed that the EVH1 domain of yeast Dcp1 recognizes a novel consensus proline-rich sequence (PRS) present in Edc1 and Edc2. Upon binding to Dcp1, these coactivators dramatically stimulate decapping, affecting both mRNA binding and the rate of the catalytic step. These observations suggest that a crucial function of Dcp1 is to couple the binding of the coactivators to substrate recognition and activation of Dcp2.

The mechanism of how a decapping enzyme is recruited and activated upon PTC recognition during NMD remains poorly understood. It has been shown that both yeast and human Upf1 can coimmunoprecipitate or show two-hybrid interaction with Dcp1a or Dcp2, but in no case has a direct interaction been demonstrated (He and Jacobson, 1995, 2001; Lykke-Andersen, 2002; Fenger-Grøn et al., 2005; Isken et al., 2008). These observations suggest that the decapping enzyme is recruited to the PTC-containing mRNA by Upf1 through either direct or indirect protein-protein interactions. Recently, Cho et al. (2009) showed that human PNRC2 is a Dcp1a- and Upf1-interacting protein and interacts preferentially with the hyperphosphorylated Upf1, thereby recruiting hyperphosphorylated Upf1 into cytoplasmic processing bodies (P-bodies). Accordingly, downregulation of endogenous PNRC2 abrogates NMD, and artificially tethering PNRC2 downstream of a normal stop codon promotes NMD. These results suggest that PNRC2 mediates the crosstalk between Upf1-containing NMD machinery and the decapping complex by bridging the interaction between Dcp1a and Upf1.

PNRC2 is a nuclear receptor coactivator that contains a proline-rich Src homology domain 3 (SH3)-binding motif and a short hydrophobic motif LXXLL called the NR-box (Figure 1A) (Zhou and Chen, 2001; Zhou et al., 2000, 2006). Like its homolog nuclear receptor coregulatory protein 1 (PNRC1), PNRC2 interacts with many nuclear receptors through its SH3-binding motif (Zhou and Chen, 2001; Zhou et al., 2000, 2006). Thus, PNRC2 is a bifunctional protein that both regulates transcription and promotes mRNA decay through NMD. Consistent with these broad roles, PNRC2 has also been implicated in energy balance (Zhou et al., 2008), activating aromatase in breast tumors (Rajhans et al., 2008) and adipogenesis (Cho et al., 2012). Despite this importance, how PNRC2 interacts with Upf1 or Dcp1a and how that interaction can promote decapping have not been elucidated.

In this study, we determined the crystal structure of the EVH1 domain of human Dcp1a in complex with PNRC2 at a resolution of 2.6 Å. The structure shows that the PRS region, including part of the SH3-binding motif in PNRC2, is bound to the EVH1 domain of Dcp1a by a distinct recognition mechanism. Mutations disrupting the interaction of PNRC2 with Dcp1a abolished its P-body localization and the rapid degradation of tethered mRNA. Isothermal titration calorimetry (ITC) assays show that the NR-box of PNRC2 mediates the interaction with the hyperphosphorylated Upf1. Decapping assays show that either

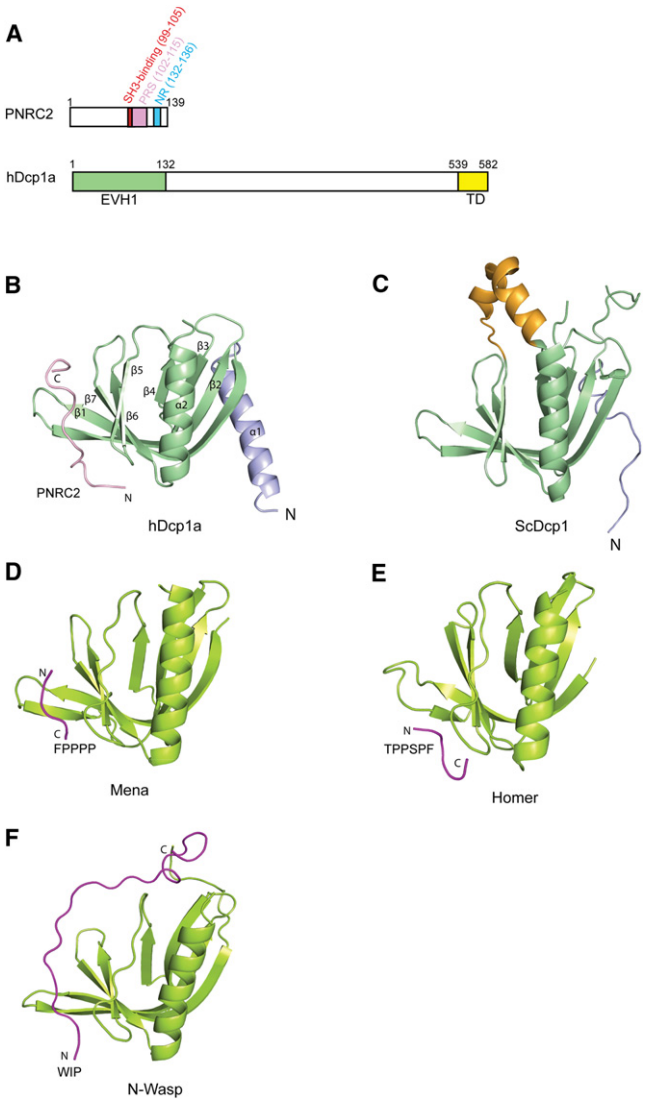

Figure 1. Comparison of Dcp1aEVH1 with EVH1 Domains from ScDcp1, Mena, Homer, and N-Wasp

(A) Schematic diagrams of domain organization of PNRC2 and hDcp1a. SH3-binding motif, PRS region and the NR box of PNRC2 are colored in red, pink, and cyan, respectively, whereas the EVH1 and the trimerization domains are shown in pale green and yellow.

(B) Structure of Dcp1aEVH1 (pale green) in complex with PNRC2 (pink) with secondary elements labeled and the N-terminal helix colored in blue.

(C) Structure of ScDcp1 (pale green) with the N-terminal region and the insertion helices shown in blue and orange, respectively.

(D) Structure of Mena EVH1 domain (lemon) in complex with the FPPPP peptide from ActA (magenta).

(E) Structure of the Homer EVH1 domain (lemon) in complex with TPPSPF peptide from mGluR (magenta).

(F) NMR structure of N-Wasp EVH1 (lemon) in complex with WIP peptide (magenta). Figures 1B–1F and 2 and Figure S1 were produced using PyMOL.

PNRC2 or Dcp1a alone stimulates decapping in vitro and the Dcp1a/PNRC2 complex synergistically enhanced the decapping activity of Dcp2. These results reveal the molecular basis of PNRC2-mediated association between the NMD machinery and the decapping complex and how PNRC2 can directly stimulate mRNA degradation.

RESULTS

Structure Determination

The EVH1 domain of human Dcp1a (designated as Dcp1aEVH1) (residues 1–130; Figure 1A) in complex with human PNRC2 (residues 1–121, designated as PNRC2ΔNR) were screened for crystallization conditions and yielded diffraction quality crystals. The protein complex was crystallized in space group *I*222, with two complexes per asymmetric unit (AU). The structure was solved by single-wavelength anomalous dispersion method at a resolution of 2.6 Å, using data obtained from selenomethionine (SeMet)-substituted crystal. Residues 1–130 of Dcp1aEVH1 and a stretch of PNRC2 polypeptide chain comprising 14 residues (residues 102 to 115) are visible in the electron density map with the rest of the residues in PNRC2 (residues 1–101 and residues 116–121) assumed to be disordered as there is no interpretable electron density for these regions. The final model contains two copies of Dcp1aEVH1 (chains A and B) complexed with the PNRC2 peptide (residues 102–115; chains C and D) with no major differences (root-mean-square deviation [rmsd] of 0.30 Å for all the equivalent Cα atoms). As chains A and C are more complete than chains B and D, the subsequent analysis reported here is based on chains A and C only.

Overall Structure Description

The overall structure of Dcp1aEVH1 (Figure 1B) is similar to that observed for *Saccharomyces cerevisiae* Dcp1 (ScDcp1) and for Mena, Homer, and N-WASP (Figure 1). Structural comparison of Dcp1aEVH1 with ScDcp1 (She et al., 2004; rmsd of ∼1.28 Å for all equivalent Cα atoms) reveals two notable differences between these two structures. First, two short helices, which are located at one of the two species-specific insertions (She et al., 2004), are present in ScDcp1 but absent in Dcp1aEVH1. Second, the N-terminal region of ScDcp1 forms a 3_{10}-helix plus an extended polypeptide, whereas in Dcp1aEVH1 this region is a long α-helix, which is similar to the long N-terminal α-helix observed in the structure of *Schizosaccharomyces pombe* Dcp1 bound to Dcp2 (She et al., 2008). The PNRC2 peptide adopts a largely extended conformation and contacts a concave groove formed by stands β1, β2, β5, β6, and β7 of Dcp1aEVH1, which includes the canonical PRS binding site observed in other EVH1 domains (see below).

The Dcp1aEVH1-PNRC2 Interface

The surface of Dcp1aEVH1 for the PNRC2 peptide binding consists of two hydrophobic pockets with Trp45 and Leu96 bridging their link (Figure 2A). The first pocket (designated as hydrophobic pocket 1), which corresponds to patch 1 of ScDcp1 (She et al., 2004), is made up of the side chains of conserved residues Tyr36, Trp45, Phe94, Leu96, and Trp108, whereas the second pocket (designated as hydrophobic pocket 2) is formed by the side chains of Phe38, Trp45, Leu96, Ile104, and the methylene groups of Glu87, Gln89, and Arg98. The N- and C-terminal portions of the PNRC2 peptide contact hydrophobic pockets 1 and 2, respectively, whereas its middle portion containing the sequence LPKP docks at the ridge formed by Trp45 and Leu96 through multiple Van der Waals (VDW) contacts. The LPKP motif adopts a polyproline II (PPII) conformation (a left-handed helix with three residues per turn) as observed in other EVH1-pepide complexes (Ball et al., 2002; see below). Importantly, one of these two regions (pocket 1) of Dcp1a that interact with PNRC2 is the same region of Dcp1 shown in yeast to be important for decapping and for binding to the decapping activator, Edc1 (Borja et al., 2011; She et al., 2004), suggesting that these are conserved interaction sites for a variety of decapping activators in numerous species (see below).

The interactions of the PNRC2 peptide with Dcp1aEVH are predominantly hydrophobic in nature, supplemented by VDW contacts and hydrogen bonding (Figure 2A; Figure S1 available online). Specifically, beginning from the N-terminal portion of the PNRC2 peptide, Pro102 forms stacking interactions with the side chain of Trp108 of Dcp1aEVH1, whereas Ser103 makes multiple VDW contacts with Tyr36, Phe94, and Trp108 of Dcp1aEVH1, in addition to the hydrogen bond formed between its carbonyl oxygen and the hydroxyl group of Tyr36 in Dcp1aEVH1. In the LPKP motif of the middle portion of the PNRC2 peptide, Leu107 and P108 protrudes into the hydrophobic pocket 1 and makes multiple hydrophobic interactions and two VDW contacts with residues Tyr36, Trp45, Phe94, and Ser106 of Dcp1aEVH1. In addition, the carbonyl oxygen of Pro108 is hydrogen-bonded to the indole nitrogen of Trp45 in Dcp1aEVH1. P110 in the LPKP motif contacts residues Phe38, Trp45, Leu96, and Ile104 in hydrophobic pocket 2 through multiple hydrophobic interactions, whereas Lys109 is exposed to the solvent region and forms a hydrogen bond with the carbonyl oxygen of Asn43. In the C-terminal portion of the PNRC2 peptide, the key residue that interacts with Dcp1aEVH1 is Trp114. This residue inserts its side chains deeply in hydrophobic pocket 2 and makes hydrophobic interactions with the side chains of Leu96 and Ile104 as well as the methylene groups of Glu87 and Arg98. In addition, the indole nitrogen of Trp114 is hydrogen-bonded to the OE1 atom of Glu87. Most of the residues involved in the Dcp1aEVH1-PNRC2 interface are highly conserved, therefore underlining their important roles in the interaction between Dcp1a and PNRC2 (Figures S2 and S3).

PNRC2 Recognition by Dcp1aEVH1

Several lines of evidence suggest that the PNRC2 peptide may bind to Dcp1aEVH via a novel recognition mechanism. First, the PNRC2 peptide does not share common motifs with the PRS ligands in other EVH1 domains, and its length (14 residues) is more than twice as long as the minimal PRS peptide (six residues) sufficient for Mena or Homer EVH1 recognition but is shorter than the Wasp Inhibitor Peptide (WIP; 25 residues) that binds to N-Wasp EVH1 (Ball et al., 2002). Third, in the structure of Dcp1aEVH1 complexed with the PNRC2 peptide, the buried surface (∼1,450 $Å^2$) is more than twice that of Mena (Prehoda et al., 1999; ∼710 $Å^2$) or Homer (Beneken et al., 2000; ∼560 $Å^2$) in complex with its respective PRS peptide but is smaller than that of the N-Wasp EVH1 with bound WIP peptide (Volkman et al., 2002; ∼2,130 $Å^2$). Fourth, as shown in Figure 2,

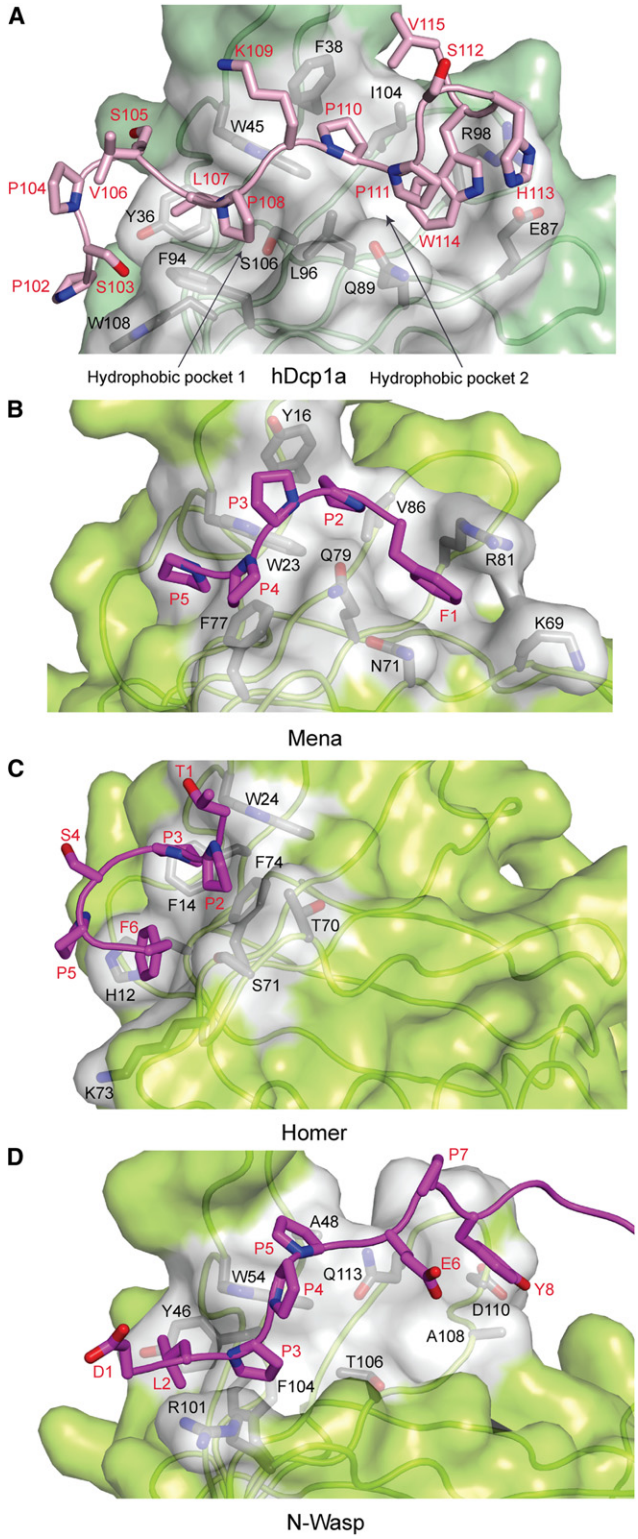

Figure 2. Surface Views of the Interfaces between the EVH1 Domains and Their PRS Ligands

Residues involved in the interfaces are labeled and shown as stick models. The surface utilized by the EVH1 domain for recognizing the PRS ligand is shown in light gray, whereas the coloring scheme for the rest of the surface is as in Figure 1.

a set of four aromatic residues (Tyr36, Phe38, Trp45, and Phe94) in Dcp1aEVH1 is involved in the recognition of the PNRC2 PRS peptide. In contrast, a different set of three aromatic residues in other EVH1 domains (Tyr16, Trp23, and Phe77 in Mena; Phe14, Trp24, and Phe74 in Homer and Tyr46; and Trp54 and Phe104 in N-Wasp) is responsible for recognizing the PRS ligands.

Although the binding of PNRC2 to Dcp1aEVH1 retains the characteristics that are common to all classes of previously characterized EVH1 domains upon binding to their respective PRS peptides (Figure 2), that is, the proline-rich motif of PNRC2, LPKP, binds to the same canonical aromatic surface utilized by all classes of EVH1 domain to recognize their peptide ligands and adopts a polyproline II (PPII) helical conformation, several features indicated that the interaction between Dcp1aEVH1 and PNRC2 appears to encompass the elements that were previously thought to be unique to all three classes of EVH1 domain. First, the binding of the LPKP motif of the PNRC2 peptide to Dcp1aEVH1 resembles that of the FPPPP peptide bound to the Mena EVH1 (Prehoda et al., 1999). Moreover, the stacking interaction between the methylene group of Arg98 in Dcp1a and Trp114 in the C-terminal portion of the PNRC2 peptide (Figure 2A; Figure S1) is similar to the interaction between Arg81 of Mena and Phe1 of the FPPPPT peptide (Figure 2B). Second, the N-terminal portion of the PNRC2 peptide binds to the edge of the hydrophobic pocket 1 of Dcp1aEVH1 in a conformation similar to that observed for the mGlu peptide bound to the Homer EVH1 domain (Beneken et al., 2000) (Figures 2A and 2C). Third, the PNRC2 peptide binds to Dcp1aEVH1 in the same orientation as the WIP peptide bound to the N-Wasp EVH1 but in a reverse orientation as compared to the PRS ligands bound to Mena and Homer (Volkman et al., 2002) (Figure 1). Taken together, these results indicate that Dcp1aEVH1 recognizes PNRC2 via a distinct recognition mechanism.

Mutational Effects on the PNRC2/Dcp1a Interaction, P-Body Localization and NMD

To delineate the role of the interface between Dcp1aEVH1 and PNRC2 in vivo, we mutated residues in the Dcp1aEVH1/PNRC2 interface and examined the effects of these mutations on their interactions as well as on P-body localization and the ability of PNRC2 to stimulate mRNA degradation. Yeast two-hybrid assays identified one mutation L96A in Dcp1a that abolished the binding to PNRC2 and four Dcp1a mutations Y36A, W45A, F94A, and R98A that showed reduced binding to PNRC2 (Figure 3A). Moreover, in PNRC2 the mutations W114A and K109A abrogated the binding of PNRC2 to Dcp1a, whereas mutation P108A substantially reduced binding to

(A) Surface representation of Dcp1aEVH1 with bound PNRC2 peptide (residues 102–115). The LPKP motif of PNRC2 in a PPII conformation docks against the conserved aromatic surface spanning from hydrophobic pocket 1 to 2.
(B) Surface representation of the Mena EVH1 domain in complex with the FPPPP peptide.
(C) Surface representation of the Homer EVH1 domain in complex with the TPPSPF peptide.
(D) Surface representation of the N-Wasp EVH1 domain with the bound WIP peptide.
See also Figures S1–S3.

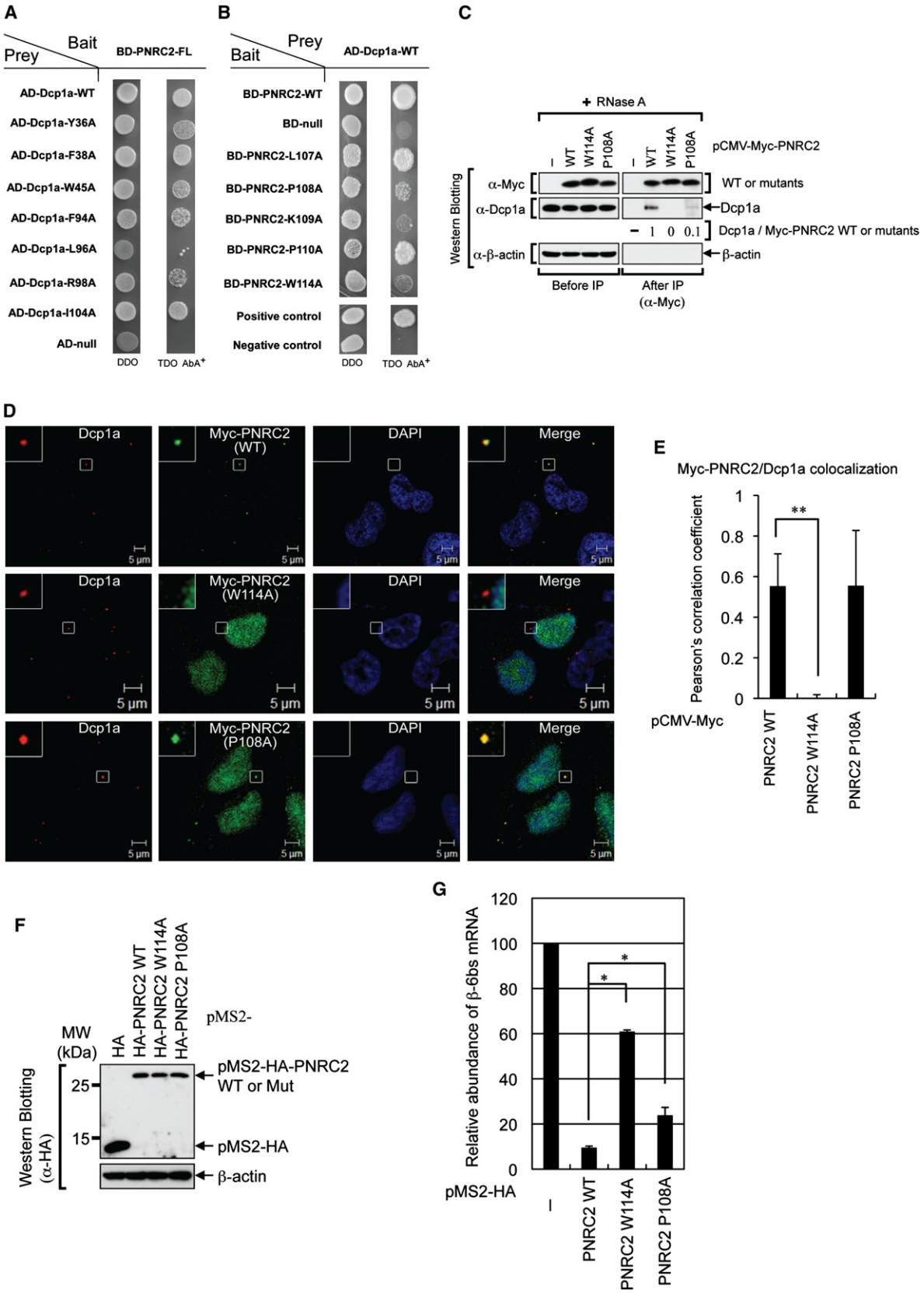
A
Prey
Bait
BD-PNRC2-FL
AD-Dcp1a-WT
AD-Dcp1a-Y36A
AD-Dcp1a-F38A
AD-Dcp1a-W45A
AD-Dcp1a-F94A
AD-Dcp1a-L96A
AD-Dcp1a-R98A
AD-Dcp1a-I104A
AD-null
DDO
TDO AbA+
B
Prey
Bait
AD-Dcp1a-WT
BD-PNRC2-WT
BD-null
BD-PNRC2-L107A
BD-PNRC2-P108A
BD-PNRC2-K109A
BD-PNRC2-P110A
BD-PNRC2-W114A
Positive control
Negative control
DDO
TDO AbA+
C
+ RNase A
pCMV-Myc-PNRC2
- WT W114A P108A - WT W114A P108A
Western Blotting
α-Myc
WT or mutants
α-Dcp1a
Dcp1a
- 1 0 0.1
Dcp1a / Myc-PNRC2 WT or mutants
α-β-actin
β-actin
Before IP
After IP
(α-Myc)
D
Dcp1a
Myc-PNRC2 (WT)
DAPI
Merge
Myc-PNRC2 (W114A)
Myc-PNRC2 (P108A)
5 μm
E
Myc-PNRC2/Dcp1a colocalization
Pearson's correlation coefficient
1
0.8
0.6
0.4
0.2
0
**
pCMV-Myc
PNRC2 WT
PNRC2 W114A
PNRC2 P108A
F
MW (kDa)
HA
HA-PNRC2 WT
HA-PNRC2 W114A
HA-PNRC2 P108A
pMS2-
25
15
pMS2-HA-PNRC2 WT or Mut
pMS2-HA
β-actin
Western Blotting (α-HA)
G
Relative abundance of β-6bs mRNA
120
100
80
60
40
20
0
*
*
pMS2-HA
-
PNRC2 WT
PNRC2 W114A
PNRC2 P108A

Dcp1a (Figure 3B). Consistent with these results, coimmunoprecipitation assays showed that PNRC2 mutants (PNRC2 W114A, and PNRC2 P108A) fail to or very weakly interact with Dcp1a, compared to PNRC2 WT (Figure 3C).

These mutations suggest that PNRC2 and other coactivators bind Dcp1/Dcp1a in a similar manner. For example, the mutation of Tyr47 to alanine in ScDcp1 (equivalent to Tyr36 in Dcp1a) disrupted its binding to the Edc1 PRS peptide (Borja et al., 2011). Moreover, and analogous to the Pro118 and Trp114 mutations in PNRC2, the corresponding residues in yeast Edc1 (Pro170) (Borja et al., 2011) and SMAD4 (Trp302) (Bai et al., 2002) have been found to be essential for binding to ScDcp1 and Dcp1a, respectively.

To check whether mutations of P108A and W114A in PNRC2 affect its P-body localization, the endogenous Dcp1a was used as a P-body marker. As shown in Figures 3D and 3E, the signal from wild-type (WT) PNRC2 almost completely overlapped with that from Dcp1a, indicating PNRC2 is localized to P-bodies. On the other hand, PNRC2(W114A), which disrupts the interaction with Dcp1a, was mainly localized to nucleus, whereas PNRC2(P108A), with reduced Dcp1a interaction, was localized to both P-bodies and nucleus. Thus, the interaction of PNRC2 with Dcp1a is required for its localization to P-bodies.

To test if the interaction of PNRC2 with Dcp1a is required for its ability to promote mRNA degradation, we examined how the P108A and W114A mutations in PNRC2 affected its ability to promote mRNA degradation when tethered to mRNAs through the MS2 RNA binding proteins (Cho et al., 2009). As assessed by quantitative real-time RT-PCR, we observed that tethering of PNRC2(WT) strongly reduced mRNA levels, tethering of W114A and P108A mutations into PNRC2 inhibited the efficiency of mRNA degradation by 6.4- and 2.5-fold, respectively (Figures 3F and 3G). Taken together, these results indicate that the binding of PNRC2 to Dcp1a is important for its P-body localization and for PNRC2′s ability to promote mRNA degradation.

The NR Box of PNRC2 Is Required for Binding to the Phosphorylated Upf1

Yeast two-hybrid showed that the SH3-binding motif and/or the NR box in the C terminus of PNRC2 is sufficient for Upf1 binding and PNRC2 preferentially interacts with hyperphosphorylated Upf1 compared with wild-type Upf1 (Cho et al., 2009). Preferential association between hyperphosphorylated Upf1 and Dcp1a also has been reported (Isken et al., 2008), but indirect interaction cannot be ruled out as the binding result was obtained using coimmunoprecipitation. Our structure shows that the PRS region downstream of the SH3-binding motif in PNRC2 directly binds to Dcp1a, whereas Zhou et al. (2006) showed that the SH3-binding motif is essential for binding to the nuclear receptors. Thus, the binding of Upf1 to Dcp1a might be mediated by the direct association of the hyperphosphorylated Upf1 with the NR box of PNRC2.

To examine if the NR box of PNRC2 directly binds to the hyperphosphorylated Upf1, we synthesized a double-phosphorylated Upf1 peptide L(pS)QPEL(pS)QDSYLGD, which is derived from the human Upf1 C-terminal SQ-containing peptide LSQP ELSQDSYLGD. This peptide has been shown to be the best substrate phosphorylated by human SMG1 (Yamashita et al., 2001). ITC titration was used to analyze the binding of this double-phosphorylated Upf1 peptide to the protein complexes Dcp1aEVH1-PNRC2ΔNR and Dcp1aEVH1-PNRC2FL (herein the full-length PNRC2 was used). As a control, the binding of the nonphosphoryated Upf1 peptide to Dcp1aEVH1-PNRC2FL was also examined. Dcp1aEVH1-PNRC2FL binds to the double-phosphorylated Upf1 peptide with an apparent Kd of 0.21 μM (Figure 4A) and shows no binding to the nonphosphoryated Upf1 peptide (Figure 4B), whereas Dcp1aEVH1-PNRC2ΔNR in which the NR-box of PNRC2 was deleted shows no detectable binding to the phopho-Upf1 peptide (Figure 4C). Taken together, these results suggest that the NR box of PNRC2 is required for its binding to the phosphorylated Upf1.

PNRC2 and Dcp1a Synergistically Stimulate Decapping In Vitro

The C-terminal regions of Edc1 and Edc2 contain a proline-rich consensus sequence that binds to ScDcp1, thereby allowing ScDcp1 to recruit the coactivators Edc1 and Edc2 to Dcp2 for decapping stimulation (Borja et al., 2011; Schwartz et al., 2003). Sequence comparison showed that the PNRC2 peptide bound to Dcp1aEVH1 shares the characteristic of the proline-rich consensus sequence of Edc1 and Edc2 (Figure 5A),

Figure 3. Mutational Effects on the PNRC2/Dcp1a Interaction, P-Body Localization, and Degradation of the Tethered mRNA

(A and B) Yeast two-hybrid analysis of the interaction between Dcp1a and PNRC2. (A) Wild-type and seven interface mutants of Dcp1a in AD vector against PNRC2 in BD vector. (B) Wild-type and five interface mutants of PNRC2 in BD vector against Dcp1a in AD vector. The cotransformed yeast cells expressing both proteins were first selected on auxotrophic media lacking leucine, tryptophan (DDO panel), and replica-plated on highly selective media lacking histidine, leucine, and tryptophan but containing 120 ng/ml aureobasidin A (TDO AbA$^+$ panel).

(C) IPs of PNRC2 WT and its variants. HEK293T cells were transiently transfected with plasmids expressing Myc, Myc-PNRC2 WT, Myc-PNRC2 W114A, or Myc-PNRC2 P108A. Two days later, cell lysates were treated with RNase A, and then IPs were performed using α-Myc antibody. The level of coimmunoprecipitated Dcp1a was normalized to the level of immunoprecipitated Myc-PNRC2 WT, W114A, or P108A. The normalized level in the IP presence of Myc-PNRC2 WT was set to one.

(D) Immunostaining of PNRC2 WT and its deletion variants. HeLa cells were transiently transfected with plasmids expressing either Myc-PNRC2 (WT), Myc-PNRC2 (W114A), or Myc-PNRC2 (P108A). Cells were stained with a-Myc antibody and a-Dcp1a antibody. Nuclei were stained with DAPI. Enlarged images of the boxed areas are shown in the upper left corner of each image.

(E) The levels of colocalization shown in (D) were determined by Pearson's correlation coefficient. At least ten cells were analyzed in two independent experiments. Two-tailed, equal-sample variance Student's t tests were used to calculate the p values. $^{**}p < 0.01$.

(F and G) Tethering of PNRC2 WT and its deletion variants. HeLa cells were transiently cotransfected with the reporter plasmid expressing β-6bs mRNA, effector plasmid expressing MS2-fused tethering protein, and the reference plasmid expressing MUP mRNA. (F) Western blotting to show the comparable expression of MS2 fusion proteins. (G) qRT-PCR of β-6bs mRNA and MUP mRNA. The levels of β-6bs mRNA were normalized to the level of MUP mRNA. The normalized levels of β-6bs mRNA in the presence of MS2-HA were set to 100%. The columns and bars represent the means and standard deviations, respectively, obtained from three independent transfections and qRT-PCRs. $^{*}p < 0.05$.

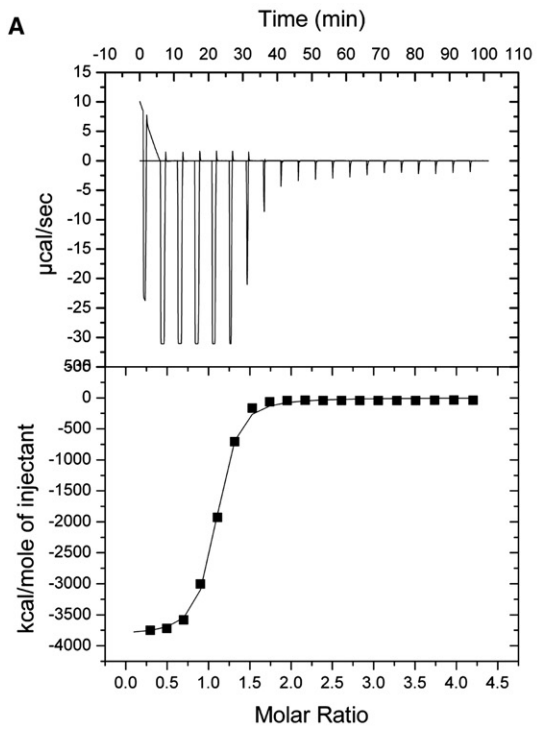

Phosphorylated Upf1 vs Dcp1aEVH1-PNRC2FL

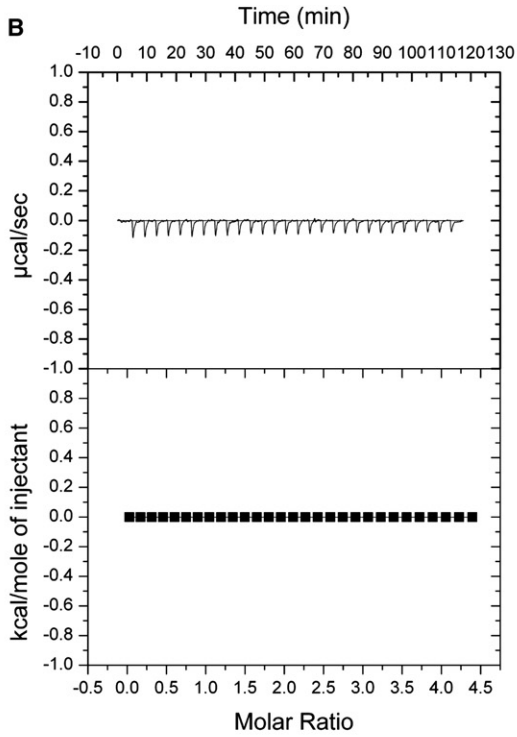

Nonphosphorylated Upf1 vs Dcp1aEVH1-PNRC2FL

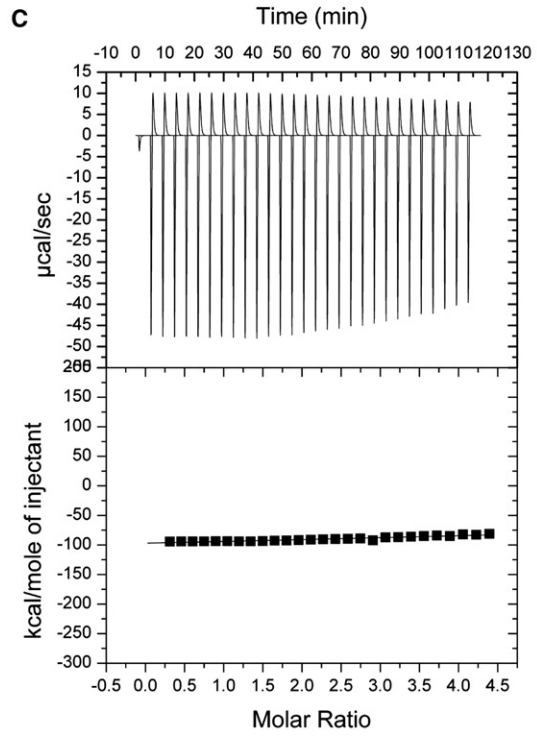

Phosphorylated Upf1 vs Dcp1aEVH1-PNRC2ΔNR

suggesting that PNRC2 may stimulate the decapping itself through Dcp1a-mediated recruitment to Dcp2.

Because ScDcp1 just contains the EVH1 domain, yet is capable of stimulating decapping in vitro (She et al., 2004, 2006; Sheth and Parker, 2006), we reasoned that the EVH1 domain alone of human Dcp1a might be sufficient to stimulate decapping in vitro. As expressing Dcp1aEVH1 or PNRC2ΔNR alone in *Escherichia coli* gave rise to insoluble protein, we coexpressed Dcp1aEVH1 and PNRC2ΔNR(W114A), a mutant showing residual binding to Dcp1aEVH1 (Figure 3B, see above). The residual interaction between Dcp1a and PNRC2ΔNR (W114A) improved the solubility of each individual protein and allowed us to purify Dcp1aEVH1 and PNRC2ΔNR(W114A) separately by attaching a His-tag to either Dcp1aEVH1 or PNRC2ΔNR(W114A) in two separate coexpression constructs and then removing the untagged protein by washes of the Ni-affinity column. SDS-PAGE gel showed that purified Dcp1aEVH1 and PNRC2ΔNR(W114A) are at least 95% pure (Figure S4).

Decapping assays showed that Dcp1aEVH1 alone stimulated decapping moderately (Figure 5B, lanes 5–7; Figure 5C, lanes 5–7), whereas PNRC2ΔNR(W114A) alone stimulated decapping strongly (Figure 5B, lanes 8–10; Figure 5C, lanes 8–10). The stronger decapping stimulation of PNRC2ΔNR(W114A) could be contributed to some extent by the trace amount of Dcp1aEVH1 that copurified with this mutant. When the Dcp1aEVH1-PNRC2ΔNR complex was added to the decapping reaction solution, the efficiency of decapping activity of human Dcp2 was markedly enhanced (Figure 5B, lanes 11–13; Figure 5C, lanes 11–13), suggesting that PNRC2 and Dcp1aEVH1 worked in a cooperative manner to stimulate Dcp2 decapping activity.

To gain insight into the mechanism by which PNRC2 stimulates decapping, we examined whether GST-Dcp2 binds to purified Dcp1aEVH1, PNRC2ΔNR(W114A), and their complex by His-tag pull-down assays. Western blotting analysis using α-GST antibody showed that the complex bound to GST-Dcp2 strongly, and PNRC2ΔNR(W114A) bound to GST-Dcp2 weakly, whereas Dcp1aEVH1 had no detectable binding to GST-Dcp2 (Figure 6A). The interaction of the complex or PNRC2ΔNR (W114A) with GST-Dcp2 is not mediated by GST as GST alone had no interaction with the proteins used here (Figure 6A). Consistent with the in vitro binding results, downregulation of endogenous PNRC2 using small interfering RNA (siRNA) (Figure 6B) reduced the interaction between endogenous Dcp1a and FLAG-Dcp2 by about 3-fold (Figure 6C), suggesting that PNRC2 plays a role in mediating the association between Dcp1a and Dcp2. Taken together, these results indicate that PNRC2 is a bona fide decapping coactivator and acts synergistically with Dcp1a to activate decapping in addition to its adaptor role in NMD.

DISCUSSION

In this study, we have shown that the PNRC2 peptide binds to Dcp1aEVH1 via a distinct recognition mechanism. Interestingly, part (PSPS) of the SH3-binding motif (residues 99–105) binds to the Dcp1aEVH1 surface outside the canonical PRS binding groove with the side chains of the proline residues (Pro102 and Pro104) exposed to the solvent region (Figure 2A), suggesting that this motif does not contribute much to the binding specificity toward Dcp1a. Consistent with this observation, the SH3 binding motif of PNRC2 has been shown to be essential for its interaction with the nuclear receptors (Zhou et al., 2006). The LPKP motif of the PNRC2 peptide binds to the canonical PRS binding site and adopts a PPII conformation with Pro108 being one of the key specificity determinants (Figures 2A and 3B). In the C-terminal portion of the PNRC2 peptide, Trp114, a second critical residue for binding specificity, protrudes deeply into a hydrophobic pocket on the Dcp1a surface (Figure 2A). Consistent with these observations, point mutations of these two residues in PNRC2 showed strong defects in Dcp1a binding, P-body localization, and degradation of tethered mRNAs (Figure 3).

Our decapping assays show that both Dcp1aEVH1 and PNRC2 in isolation simulate decapping and, more importantly, that PNRC2 works in synergy with Dcp1a to promote the decapping activity of Dcp2 (Figures 5B and 5C). In yeast, Edc1 and Edc2 stimulate decapping through ScDcp1-mediated recruitment to Dcp2, as Dcp1 and Dcp2 physically interact with each other to form the holo-decapping enzyme (Beelman et al., 1996; Sakuno et al., 2004; Steiger et al., 2003). However, in mammals, the interaction of Dcp1a with Dcp2 has been reported to be mediated by the adaptor protein Edc4 (Hedls), which itself is a decapping coactivator (Fenger-Grøn et al., 2005), suggesting that the recruitment of PNRC2 to Dcp2 is not directly mediated by Dcp1a. Consistent with this notion, our pull-down and western blotting analyses indicate that PNRC2 directly binds to Dcp2 albeit with low affinity, whereas the binding of Dcp1a to Dcp2 is mediated by PNRC2 (Figure 6). Therefore, in contrast to the mode of action of Edc1 and Edc2 (Borja et al., 2011), PNRC2 stimulates decapping through direct binding to Dcp2, whereas Dcp1a stimulates decapping through PNRC2-mediated recruitment to Dcp2. Given that Upf1 phosphorylation is a key step in PTC recognition during NMD and PNRC2 preferentially binds the hyperphosporylated Upf1 (Cho et al., 2009), the direct interactions of PNRC2 with both Dcp1a and Dcp2 would link the mRNA surveillance machinery with the decapping complex after Upf1 phosporylation, therefore transducing the signal of PTC recognition to the decapping complex and triggering mRNA decapping.

Two recent reports have demonstrated that transcription factors and DNA promoters can directly influence the relative stablility of transcripts that they produce (Bregman et al., 2011; Trcek et al., 2011), suggesting that transcription and mRNA decay are coordinated to each other to regulate the level of an mRNA. In further support of these observations, mRNA decapping factors Dcp1a, Dcp2, and Edc3 and exonuclease Xrn2 were reported to function in widespread premature termination of RNA polymerase II transcription (Brannan et al., 2012). Dcp1a (also called SMIF) has been shown to function as a crucial

Figure 4. The NR Box of PNRC2 Is Required for Binding to the Phosphorylated Upf1 Peptide

(A and B) ITC titrations of the double-phosphorylated and nonphosphorylated Upf1 peptides to the Dcp1aEVH1-PNRC2FL complex, respectively.

(C) Titration of the double-phosphorylated Upf1 peptide to the Dcp1aEVH1-PNRC2ΔNR complex. The upper panels show the binding isotherms, and the lower panels show the integrated heat for each injection fitted to a single-site model.

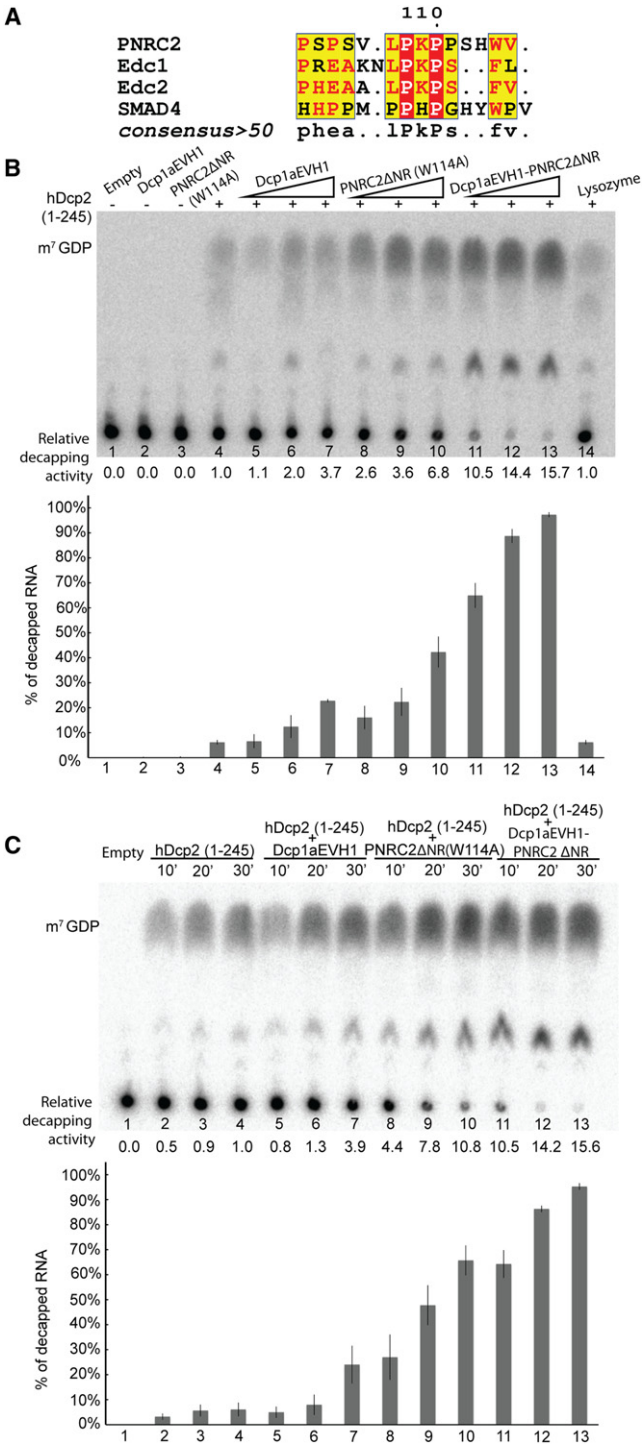

Figure 5. Dcp1a and PNRC2 Synergistically Stimulate the Decapping Activity of hDcp2

(A) Sequence alignment of the proline-rich region of PNRC2 (residues 102–115) with the proline-rich sequences of Edc1 (residues 163–175) and Edc2 (residues 134–145) from *S. cerevisiae* and Smad4 (residues 290–304) from *Homo sapiens*.

(B) Upper panel: Effects of Dcp1aEVH1, PNRC2ΔNR(W114A), and Dcp1aEVH1-PNRC2ΔNR on the decapping activity of hDcp2(1–245). The enhanced decapping activities were quantified using the amount of cap-labeled RNA relative to that of hDcp2(1–245) alone (lane 4) from three independent measurements with the bars representing standard deviations from the mean. Lower panel: Quantification of the stimulation effects shown in the upper panel. Student's t test was used to assess the statistically significant difference of the decapping activity of hDcp2(1–245) before (lane 4) and after addition of the indicated proteins (lanes 7, 10, and 13) with a p value of less than 0.01.

(C) Upper panel: Time-course decapping reactions with the indicated proteins. The proteins were incubated with cap-labeled RNA at room temperature for the time points indicated. Lower panel: Quantification of the stimulation effects shown in the upper panel. Student's t test was used to assess the statistically significant difference of the decapping activity of hDcp2(1–245) before (lane 4) and after addition of the indicated proteins (lanes 7, 10, and 13) with a p value of less than 0.05. The columns and bars represent the means and standard deviations, respectively, calculated from three replicate experiments.

See also Figure S4.

transcriptional coactivator in TGFβ signaling (Bai et al., 2002). In this study, we demonstrate that PNRC2 stimulates mRNA decapping. Therefore, both Dcp1a and PNRC2 are bifunctional proteins to regulate both decapping and transcription by acting as a decapping activator and a transcriptional coactivator.

Dcp1a binds to the C-terminal proline-rich linker region of SMAD4 using its EVH1 domain (Bai et al., 2002). A Trp residue (Trp302) in this proline-rich linker region of SMAD4 is critical for binding to SMIF and its transcriptional activity. Sequence analysis shows that the PNRC2 peptide and the proline-rich linker region of SMAD4 share a consensus sequence with Trp302 in SMAD4 corresponding to Trp114 in PNRC2 (Figure 5A). The conservation of this aromatic residue in the PRS peptide between PNRC2 and SMAD4 can be extended to Edc1 and Edc2 as both proteins contain a Phe in the consensus PRS sequence (Figure 5A). These observations suggest that the presence of an aromatic residue (Phe or Trp) in the C terminus of the PRS peptide could be a general feature for binding to the EVH1 domain of Dcp1 proteins. Given that PNRC2, Edc1, and Edc2 stimulate decapping, it would be interesting to investigate in the future whether SMAD4 is a decapping activator.

EXPERIMENTAL PROCEDURES

Structure Determination

Human PNRC2ΔNR (residues 1–121) and human Dcp1aEVH1 (residues 1–130) were coexpressed in *E. coli* and purified by TALON metal affinity resin, Mono Q, and Superdex-200 gel filtration columns. Crystals of the Dcp1a/PNRC2 complex were grown at 15°C by hanging drop vapor diffusion method. Equal volumes of protein and crystallization reagents (27% [w/v] PEG 3350, 0.15 M ammonium acetate, 0.1 M Bis Tris [pH 5.5], and 0.01 M Hexamine cobalt [III] chloride) were mixed. Before data collection, the crystals were transferred to the mother liquor containing 15% glycerol and flash frozen in liquid nitrogen.

Diffraction data were collected at the peak wavelength of selenium absorption edge (λ = 0.9798 Å) at beamline ID23-1, European Synchrotron Radiation Facility (ESRF), Grenoble, France. The best diffraction volumes of the crystals were defined using diffraction cartography (Bowler et al., 2010). The SAD data were processed using the CCP4 suite (Collaborative Computational Project, Number 4, 1994). The crystals belong to space group *I*222 with two molecules in the asymmetric unit (AU). Six out of seven selenium sites were found by SnB (Miller et al., 1994). SHARP (de la Fortelle and Bricogne, 1997) was used to further refine the Se sites and estimate the phase. After solvent flattening, a partial model built from RESOLVE was used for manual model building with program COOT (Emsley and Cowtan, 2004). The model was refined with CNS (Brünger et al., 1998), REFMAC (Murshudov et al., 1997), and Phenix (Adams et al., 2010) with the use of TLS (Painter and Merritt, 2006a, 2006b). Water molecules were added using Arp/Warp solvent (Perrakis et al., 2001)

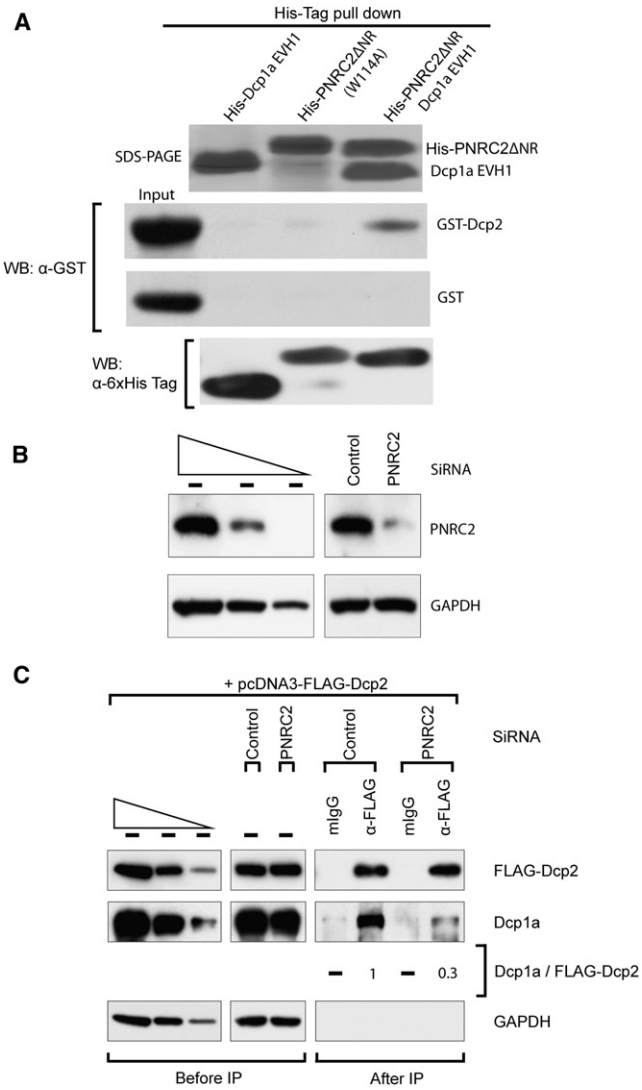

Figure 6. Interactions of PNRC2 and Dcp1a with Dcp2

(A) PNRC2ΔNR(W114A) and the Dcp1aEVH1-PNRC2ΔNR complex, but not Dcp1aEVH1, bind to Dcp2 with weak and strong affinities, respectively. Purified His-Dcp1aEVH1, His-PNRC2ΔNR(W114A), and the Dcp1a EVH1-His-PNRC2ΔNR complex (toppanel) were separately precipitated with GST-Dcp2 (middle upper panel) or the GST alone (middle lower panel) and analyzed by western blotting with anti-GST antibody. Coeluted His-tagged proteins were analyzed by western blotting with anti-His-tag antibody (bottom panel). Note that His-Dcp1aEVH1 and His-PNRC2ΔNR(W114A) migrate slower than the corresponding proteins in the complex probably (first and fourth panels) because of the presence of His-tag attached to Dcp1aEVH1 and the W114A mutation in PNRC2ΔNR, respectively, as the protein identities of the samples have been confirmed by mass spectrometry analysis.

(B and C) IPs of FLAG-Dcp2 using the extracts of HEK293T cells depleted of endogenous PNRC2. HEK293T cells were transfected with PNRC2 siRNA or nonspecific Control siRNA. Two days after transfection, cells were transiently retransfected with plasmids expressing FLAG-Dcp2. (B) Western blotting of PNRC2. To demonstrate the quantitativity of western blotting, 3-fold serial dilutions of total-cell extracts were loaded in the three left-most lanes. (C) IP of FLAG-Dcp2. IP was performed using α-FLAG antibody or mouse IgG as a control. The levels of coimmunopurified endogenous Dcp1a were normalized to the level of immunopurified FLAG-Dcp2. The normalized level in presence of control siRNA was set to one.

See also Figure S4.

Table 1. X-Ray Data Collection, Phasing, and Refinement Statistics

Data Collection	Dcp1aEVH1-PNRC2ΔNR
Wavelength (Å)	0.9793
Resolution limit (Å)	2.60
Space group	I222
Unit cell dimensions	
a, b, c (Å)	77.20, 98.82, 107.01
α, β, γ (°)	90, 90, 90
Reflections	
Measured	42,138
Unique	12,401
Completeness (%)	98.4 (91.0)
Redundancy	3.4
I/σ	19.1 (4.9)
R_{merge} [a]	0.037 (0.166)
Phasing statistics	
Number of Se sites	6
R_{cullis} [b]	0.69
Figure of merit	
Before density modification	0.30
After density modification	0.82
Refinement	
Resolution range (Å)	20–2.6
Number of atom	
Protein	2,082
Water	67
R_{work} [c] (%)	23.4
R_{free} [d] (%)	28.5
Rmsd	
Bond lengths (Å)	0.008
Bond angles (°)	1.24
Ramachandran plot	
Allowed (% residues)	99.1
Generously allowed (% residues)	0.9
Disallowed (% residues)	0

Values in parentheses indicate the values in the highest resolution shell.

[a] $R_{merge} = \Sigma|I_j - \langle I \rangle| / \Sigma I_j$, where I_j is the intensity of an individual reflection, and $\langle I \rangle$ is the average intensity of that reflection.

[b] $R_{cullis} = \Sigma_h||F_{PH} - F_H| - |F_H||/ \Sigma_h|F_{PH} - F_H|$.

[c] $R_{work} = \Sigma||F_o - F_c||/ \Sigma|F_c|$, where F_o denotes the observed structure factor amplitude, and F_c denotes the structure factor amplitude calculated from the model.

[d] R_{free} is similar to R_{work} but calculated with 10.0% of randomly chosen reflections that are omitted from the refinement.

and further refined by Phenix. The final model has good stereochemistry with a free R factor of 28.5% and an R factor of 23.4%. Data collection and refinement statistics are shown in Table 1.

Immunostaining

HeLa cells were fixed with 2% paraformaldehyde (Merck, Whitehouse Station, NJ, USA) in PBS for 10 min and permeabilized with 0.5% Triton X-100 in PBS for 10 min. The permeabilized cells were incubated in blocking buffer

(1.5% BSA in PBS) for 1 hr and then incubated with either α-Myc antibody (Calbiochem, Darmstadt, Germany) or α-Dcp1a antibody (Sigma-Aldrich, St. Louis, MO, USA) for 1 hr. The antibodies were detected with either fluorescein- or rhodamine-conjugated secondary antibodies (Pierce, Thermo Fisher Scientific Inc., Rockford, IL, USA). Nuclei were stained with DAPI (Biotium, Hayward, CA, USA). Cells were observed with a ZEISS confocal microscope (LSM510 META). The level of colocalization was quantitated by calculating the Pearson's correlation coefficient with LSM510 META software.

Immunoprecipitation

HEK293T cells were transiently transfected with PNRC2 siRNA (Cho et al., 2009) or nonspecific control siRNA (Kim et al., 2005) using Oligofectamine (Invitrogen, Carlsbad, CA, USA). Two days after siRNA transfection, cells were retransfected with plasmid expressing FLAG-Dcp2 using the calcium phosphate method. IP was perfomed using indicated antibody as previously described (Cho et al., 2009). Coimmunopurified proteins were analyzed by western blotting using the following antibodies: α-FLAG antibody (Sigma-Aldrich), α-Dcp1a (Cho et al., 2012), α-Myc (Calbiochem), α-β-actin (Sigma-Aldrich), and α-GAPDH (Ab Frontier, Young In Frontier Co. Ltd, Seoul, Korea).

Decapping Assays

The preparation of ^{32}P-labeled capped mRNA is described as before (She et al., 2006). The decapping buffer contains 50mM Tris-HCl (pH 7.9), 30mM ammonium nitrate and 0.2mM $MnCl_2$. For checking the stimulation of decapping, 5, 10 and 20 pmol of Dcp1aEVH1 or PNRC2ΔNR(W114A), and 2, 4 and 6 pmol of the Dcp1aEVH1-PNRC2ΔNR complex were incubated with 10 pmol of hDcp2 in the reaction buffer on ice for 1 hr before 80 fmol of the capped RNA was added. The decapping reaction was carried out at room temperature before being stopped by addition of 25 mM EDTA. Aliquots (5 μl) of the reaction products from decapping assays was spotted on polyethyleneimine-cellulose TLC plates (Sigma) and developed in 0.75M LiCl. Quantification of cap-labeled RNA was performed using a Phosphorimager.

ACCESSION NUMBERS

The coordinates and structure-factor amplitudes of the Dcp1aEVH1-PNRC2ΔNR complex have been deposited in the Protein Data Bank under the accession code 4b6h.

SUPPLEMENTAL INFORMATION

Supplemental Information includes Supplemental Experimental Procedures and four figures and can be found with this article online at http://dx.doi.org/10.1016/j.str.2012.09.009.

ACKNOWLEDGMENTS

We thank Dr. Jens Lykke-Andersen for plasmids used in the tethering experiments. This work is supported by the Agency for Science, Technology and Research in Singapore (to H.S.) and partly by Zhejiang Provincial Natural Science Foundation of China (Grant no. LZ12C05001).

Received: May 4, 2012
Revised: August 17, 2012
Accepted: September 10, 2012
Published online: October 18, 2012

REFERENCES

Adams, P.D., Afonine, P.V., Bunkóczi, G., Chen, V.B., Davis, I.W., Echols, N., Headd, J.J., Hung, L.W., Kapral, G.J., Grosse-Kunstleve, R.W., et al. (2010). PHENIX: a comprehensive Python-based system for macromolecular structure solution. Acta Crystallogr. D Biol. Crystallogr. *66*, 213–221.

Amrani, N., Dong, S., He, F., Ganesan, R., Ghosh, S., Kervestin, S., Li, C., Mangus, D.A., Spatrick, P., and Jacobson, A. (2006). Aberrant termination triggers nonsense-mediated mRNA decay. Biochem. Soc. Trans. *34*, 39–42.

Bai, R.Y., Koester, C., Ouyang, T., Hahn, S.A., Hammerschmidt, M., Peschel, C., and Duyster, J. (2002). SMIF, a Smad4-interacting protein that functions as a co-activator in TGFbeta signalling. Nat. Cell Biol. *4*, 181–190.

Ball, L.J., Jarchau, T., Oschkinat, H., and Walter, U. (2002). EVH1 domains: structure, function and interactions. FEBS Lett. *513*, 45–52.

Beelman, C.A., Stevens, A., Caponigro, G., LaGrandeur, T.E., Hatfield, L., Fortner, D.M., and Parker, R. (1996). An essential component of the decapping enzyme required for normal rates of mRNA turnover. Nature *382*, 642–646.

Behm-Ansmant, I., Rehwinkel, J., and Izaurralde, E. (2006). MicroRNAs silence gene expression by repressing protein expression and/or by promoting mRNA decay. Cold Spring Harb. Symp. Quant. Biol. *71*, 523–530.

Behm-Ansmant, I., Kashima, I., Rehwinkel, J., Saulière, J., Wittkopp, N., and Izaurralde, E. (2007). mRNA quality control: an ancient machinery recognizes and degrades mRNAs with nonsense codons. FEBS Lett. *581*, 2845–2853.

Beneken, J., Tu, J.C., Xiao, B., Nuriya, M., Yuan, J.P., Worley, P.F., and Leahy, D.J. (2000). Structure of the Homer EVH1 domain-peptide complex reveals a new twist in polyproline recognition. Neuron *26*, 143–154.

Borja, M.S., Piotukh, K., Freund, C., and Gross, J.D. (2011). Dcp1 links coactivators of mRNA decapping to Dcp2 by proline recognition. RNA *17*, 278–290.

Bowler, M.W., Guijarro, M., Petitdemange, S., Baker, I., Svensson, O., Burghammer, M., Mueller-Dieckmann, C., Gordon, E.J., Flot, D., McSweeney, S.M., and Leonard, G.A. (2010). Diffraction cartography: applying microbeams to macromolecular crystallography sample evaluation and data collection. Acta Crystallogr. D Biol. Crystallogr. *66*, 855–864.

Brannan, K., Kim, H., Erickson, B., Glover-Cutter, K., Kim, S., Fong, N., Kiemele, L., Hansen, K., Davis, R., Lykke-Andersen, J., and Bentley, D.L. (2012). mRNA decapping factors and the exonuclease Xrn2 function in widespread premature termination of RNA polymerase II transcription. Mol. Cell *46*, 311–324.

Bregman, A., Avraham-Kelbert, M., Barkai, O., Duek, L., Guterman, A., and Choder, M. (2011). Promoter elements regulate cytoplasmic mRNA decay. Cell *147*, 1473–1483.

Brünger, A.T., Adams, P.D., Clore, G.M., DeLano, W.L., Gros, P., Grosse-Kunstleve, R.W., Jiang, J.S., Kuszewski, J., Nilges, M., Pannu, N.S., et al. (1998). Crystallography & NMR system: A new software suite for macromolecular structure determination. Acta Crystallogr. D Biol. Crystallogr. *54*, 905–921.

Chang, Y.F., Imam, J.S., and Wilkinson, M.F. (2007). The nonsense-mediated decay RNA surveillance pathway. Annu. Rev. Biochem. *76*, 51–74.

Cho, H., Kim, K.M., and Kim, Y.K. (2009). Human proline-rich nuclear receptor coregulatory protein 2 mediates an interaction between mRNA surveillance machinery and decapping complex. Mol. Cell *33*, 75–86.

Cho, H., Kim, K.M., Han, S., Choe, J., Park, S.G., Choi, S.S., and Kim, Y.K. (2012). Staufen1-mediated mRNA decay functions in adipogenesis. Mol. Cell *46*, 495–506.

Chowdhury, A., and Tharun, S. (2009). Activation of decapping involves binding of the mRNA and facilitation of the post-binding steps by the Lsm1-7-Pat1 complex. RNA *15*, 1837–1848.

Collaborative Computational Project, Number 4. (1994). The CCP4 suite: programs for protein crystallography. Acta Crystallogr. D Biol. Crystallogr. *50*, 760–763.

Coller, J., and Parker, R. (2004). Eukaryotic mRNA decapping. Annu. Rev. Biochem. *73*, 861–890.

Coller, J., and Parker, R. (2005). General translational repression by activators of mRNA decapping. Cell *122*, 875–886.

de la Fortelle, E., and Bricogne, G. (1997). Maximum-likelihood heavy-atom parameter refinement for multiple isomorphous replacement and multiwavelength anomalous diffraction methods. Methods Enzymol. *276*, 472–494.

Emsley, P., and Cowtan, K. (2004). Coot: model-building tools for molecular graphics. Acta Crystallogr. D Biol. Crystallogr. *60*, 2126–2132.

Eulalio, A., Rehwinkel, J., Stricker, M., Huntzinger, E., Yang, S.F., Doerks, T., Dorner, S., Bork, P., Boutros, M., and Izaurralde, E. (2007). Target-specific requirements for enhancers of decapping in miRNA-mediated gene silencing. Genes Dev. *21*, 2558–2570.

Fenger-Grøn, M., Fillman, C., Norrild, B., and Lykke-Andersen, J. (2005). Multiple processing body factors and the ARE binding protein TTP activate mRNA decapping. Mol. Cell *20*, 905–915.

Franks, T.M., and Lykke-Andersen, J. (2008). The control of mRNA decapping and P-body formation. Mol. Cell *32*, 605–615.

He, F., and Jacobson, A. (1995). Identification of a novel component of the nonsense-mediated mRNA decay pathway by use of an interacting protein screen. Genes Dev. *9*, 437–454.

He, F., and Jacobson, A. (2001). Upf1p, Nmd2p, and Upf3p regulate the decapping and exonucleolytic degradation of both nonsense-containing mRNAs and wild-type mRNAs. Mol. Cell. Biol. *21*, 1515–1530.

He, F., Li, X., Spatrick, P., Casillo, R., Dong, S., and Jacobson, A. (2003). Genome-wide analysis of mRNAs regulated by the nonsense-mediated and 5′ to 3′ mRNA decay pathways in yeast. Mol. Cell *12*, 1439–1452.

Isken, O., and Maquat, L.E. (2007). Quality control of eukaryotic mRNA: safeguarding cells from abnormal mRNA function. Genes Dev. *21*, 1833–1856.

Isken, O., Kim, Y.K., Hosoda, N., Mayeur, G.L., Hershey, J.W., and Maquat, L.E. (2008). Upf1 phosphorylation triggers translational repression during nonsense-mediated mRNA decay. Cell *133*, 314–327.

Kashima, I., Yamashita, A., Izumi, N., Kataoka, N., Morishita, R., Hoshino, S., Ohno, M., Dreyfuss, G., and Ohno, S. (2006). Binding of a novel SMG-1-Upf1-eRF1-eRF3 complex (SURF) to the exon junction complex triggers Upf1 phosphorylation and nonsense-mediated mRNA decay. Genes Dev. *20*, 355–367.

Kim, Y.K., Furic, L., Desgroseillers, L., and Maquat, L.E. (2005). Mammalian Staufen1 recruits Upf1 to specific mRNA 3'UTRs so as to elicit mRNA decay. Cell *120*, 195–208.

Lejeune, F., Li, X., and Maquat, L.E. (2003). Nonsense-mediated mRNA decay in mammalian cells involves decapping, deadenylating, and exonucleolytic activities. Mol. Cell *12*, 675–687.

Lykke-Andersen, J. (2002). Identification of a human decapping complex associated with hUpf proteins in nonsense-mediated decay. Mol. Cell. Biol. *22*, 8114–8121.

Meaux, S., van Hoof, A., and Baker, K.E. (2008). Nonsense-mediated mRNA decay in yeast does not require PAB1 or a poly(A) tail. Mol. Cell *29*, 134–140.

Mendell, J.T., Sharifi, N.A., Meyers, J.L., Martinez-Murillo, F., and Dietz, H.C. (2004). Nonsense surveillance regulates expression of diverse classes of mammalian transcripts and mutes genomic noise. Nat. Genet. *36*, 1073–1078.

Miller, R., Gallo, S.M., Khalak, H.G., and Weeks, C.M. (1994). SnB: crystal structure determination via shake-and-bake. J. Appl. Cryst. *27*, 613–621.

Mühlemann, O., and Lykke-Andersen, J. (2010). How and where are nonsense mRNAs degraded in mammalian cells? RNA Biol. *7*, 28–32.

Mühlemann, O., Eberle, A.B., Stalder, L., and Zamudio Orozco, R. (2008). Recognition and elimination of nonsense mRNA. Biochim. Biophys. Acta *1779*, 538–549.

Murshudov, G.N., Vagin, A.A., and Dodson, E.J. (1997). Refinement of macromolecular structures by the maximum-likelihood method. Acta Crystallogr. D Biol. Crystallogr. *53*, 240–255.

Painter, J., and Merritt, E.A. (2006a). Optimal description of a protein structure in terms of multiple groups undergoing TLS motion. Acta Crystallogr. D Biol. Crystallogr. *62*, 439–450.

Painter, J., and Merritt, E.A. (2006b). TLSMD web server for the generation of multi-group TLS models. J. Appl. Cryst. *39*, 109–111.

Parker, R., and Song, H. (2004). The enzymes and control of eukaryotic mRNA turnover. Nat. Struct. Mol. Biol. *11*, 121–127.

Parker, R., and Sheth, U. (2007). P bodies and the control of mRNA translation and degradation. Mol. Cell *25*, 635–646.

Perrakis, A., Harkiolaki, M., Wilson, K.S., and Lamzin, V.S. (2001). ARP/wARP and molecular replacement. Acta Crystallogr. D Biol. Crystallogr. *57*, 1445–1450.

Prehoda, K.E., Lee, D.J., and Lim, W.A. (1999). Structure of the enabled/VASP homology 1 domain-peptide complex: a key component in the spatial control of actin assembly. Cell *97*, 471–480.

Rajhans, R., Nair, H.B., Nair, S.S., Cortez, V., Ikuko, K., Kirma, N.B., Zhou, D., Holden, A.E., Brann, D.W., Chen, S., et al. (2008). Modulation of in situ estrogen synthesis by proline-, glutamic acid-, and leucine-rich protein-1: potential estrogen receptor autocrine signaling loop in breast cancer cells. Mol. Endocrinol. *22*, 649–664.

Rebbapragada, I., and Lykke-Andersen, J. (2009). Execution of nonsense-mediated mRNA decay: what defines a substrate? Curr. Opin. Cell Biol. *21*, 394–402.

Rehwinkel, J., Letunic, I., Raes, J., Bork, P., and Izaurralde, E. (2005). Nonsense-mediated mRNA decay factors act in concert to regulate common mRNA targets. RNA *11*, 1530–1544.

Rissland, O.S., and Norbury, C.J. (2009). Decapping is preceded by 3′ uridylation in a novel pathway of bulk mRNA turnover. Nat. Struct. Mol. Biol. *16*, 616–623.

Sakuno, T., Araki, Y., Ohya, Y., Kofuji, S., Takahashi, S., Hoshino, S., and Katada, T. (2004). Decapping reaction of mRNA requires Dcp1 in fission yeast: its characterization in different species from yeast to human. J. Biochem. *136*, 805–812.

Schwartz, D., Decker, C.J., and Parker, R. (2003). The enhancer of decapping proteins, Edc1p and Edc2p, bind RNA and stimulate the activity of the decapping enzyme. RNA *9*, 239–251.

She, M., Decker, C.J., Sundramurthy, K., Liu, Y., Chen, N., Parker, R., and Song, H. (2004). Crystal structure of Dcp1p and its functional implications in mRNA decapping. Nat. Struct. Mol. Biol. *11*, 249–256.

She, M., Decker, C.J., Chen, N., Tumati, S., Parker, R., and Song, H. (2006). Crystal structure and functional analysis of Dcp2p from Schizosaccharomyces pombe. Nat. Struct. Mol. Biol. *13*, 63–70.

She, M., Decker, C.J., Svergun, D.I., Round, A., Chen, N., Muhlrad, D., Parker, R., and Song, H. (2008). Structural basis of dcp2 recognition and activation by dcp1. Mol. Cell *29*, 337–349.

Sheth, U., and Parker, R. (2006). Targeting of aberrant mRNAs to cytoplasmic processing bodies. Cell *125*, 1095–1109.

Song, M.G., and Kiledjian, M. (2007). 3′ terminal oligo U-tract-mediated stimulation of decapping. RNA *13*, 2356–2365.

Song, M.G., Li, Y., and Kiledjian, M. (2010). Multiple mRNA decapping enzymes in mammalian cells. Mol. Cell *40*, 423–432.

Steiger, M., Carr-Schmid, A., Schwartz, D.C., Kiledjian, M., and Parker, R. (2003). Analysis of recombinant yeast decapping enzyme. RNA *9*, 231–238.

Teixeira, D., and Parker, R. (2007). Analysis of P-body assembly in Saccharomyces cerevisiae. Mol. Biol. Cell *18*, 2274–2287.

Trcek, T., Larson, D.R., Moldón, A., Query, C.C., and Singer, R.H. (2011). Single-molecule mRNA decay measurements reveal promoter- regulated mRNA stability in yeast. Cell *147*, 1484–1497.

Volkman, B.F., Prehoda, K.E., Scott, J.A., Peterson, F.C., and Lim, W.A. (2002). Structure of the N-WASP EVH1 domain-WIP complex: insight into the molecular basis of Wiskott-Aldrich syndrome. Cell *111*, 565–576.

Weischenfeldt, J., Damgaard, I., Bryder, D., Theilgaard-Mönch, K., Thoren, L.A., Nielsen, F.C., Jacobsen, S.E., Nerlov, C., and Porse, B.T. (2008). NMD is essential for hematopoietic stem and progenitor cells and for eliminating by-products of programmed DNA rearrangements. Genes Dev. *22*, 1381–1396.

Wittmann, J., Hol, E.M., and Jäck, H.M. (2006). hUPF2 silencing identifies physiologic substrates of mammalian nonsense-mediated mRNA decay. Mol. Cell. Biol. *26*, 1272–1287.

Yamashita, A., Ohnishi, T., Kashima, I., Taya, Y., and Ohno, S. (2001). Human SMG-1, a novel phosphatidylinositol 3-kinase-related protein kinase, associates with components of the mRNA surveillance complex and is involved in

the regulation of nonsense-mediated mRNA decay. Genes Dev. *15*, 2215–2228.

Zhou, D., and Chen, S. (2001). PNRC2 is a 16 kDa coactivator that interacts with nuclear receptors through an SH3-binding motif. Nucleic Acids Res. *29*, 3939–3948.

Zhou, D., Quach, K.M., Yang, C., Lee, S.Y., Pohajdak, B., and Chen, S. (2000). PNRC: a proline-rich nuclear receptor coregulatory protein that modulates transcriptional activation of multiple nuclear receptors including orphan receptors SF1 (steroidogenic factor 1) and ERRalpha1 (estrogen related receptor alpha-1). Mol. Endocrinol. *14*, 986–998.

Zhou, D., Ye, J.J., Li, Y., Lui, K., and Chen, S. (2006). The molecular basis of the interaction between the proline-rich SH3-binding motif of PNRC and estrogen receptor alpha. Nucleic Acids Res. *34*, 5974–5986.

Zhou, D., Shen, R., Ye, J.J., Li, Y., Tsark, W., Isbell, D., Tso, P., and Chen, S. (2008). Nuclear receptor coactivator PNRC2 regulates energy expenditure and adiposity. J. Biol. Chem. *283*, 541–553.

